Supplementary Information

Increasing Arctic dust suppresses the reduction of ice nucleation in the Arctic lower troposphere by warming

Matsui et al.

Supplementary Figures

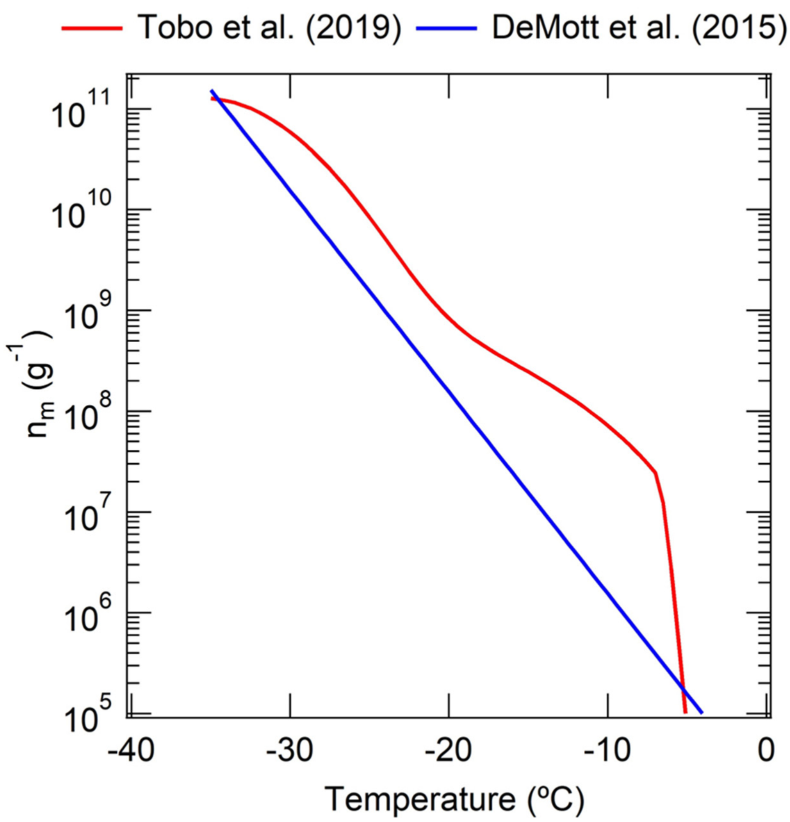

Supplementary Figure 1. Temperature dependence of ice nucleating ability (ice nucleating active site density per unit mass; n_m). The lines of n_m are shown for Arctic dust (red; Tobo et al. (2019))[1] and desert dust (blue; DeMott et al. (2015))[2]. Because the parameterization of DeMott et al. (2015) does not consider the temperature dependence of n_m directly, we derived the n_m for the parameterization of DeMott et al. (2015) using the particle size distribution of dust emissions assumed in our model[3].

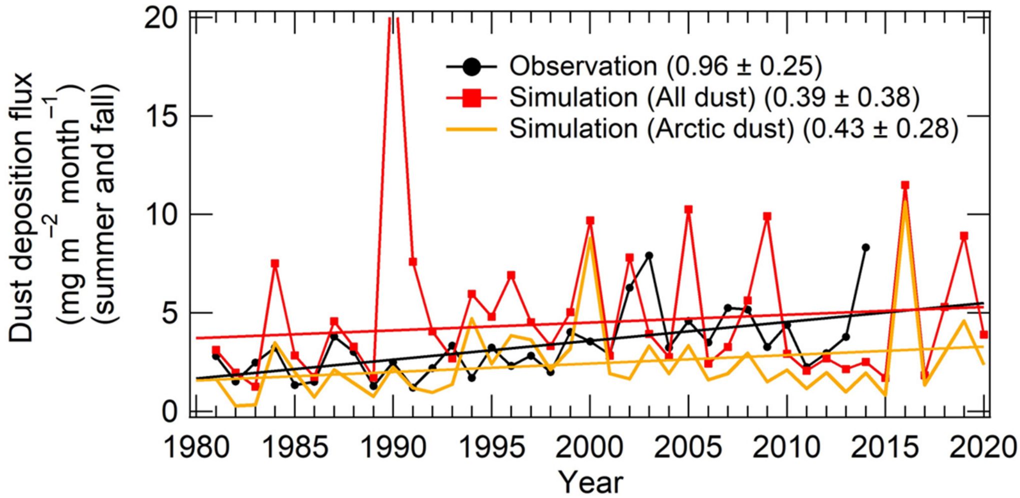

Supplementary Figure 2. Year-to-year variations of dust deposition flux at the Southeastern Greenland Dome (SE-Dome). The deposition flux in summer and fall (June−November) is shown for ice core observations[4] (black; 1981−2014) and model simulations (red and orange; 1981−2020) with their trend lines. The values in the legend indicate changes per decade in the trends (mean ± standard deviation). Summer and fall were chosen because the simulated amount of Arctic dust is high in these seasons (Fig. 4). Results of the Base simulation are shown for Arctic dust (dust emitted from >60°N) and All dust (Arctic dust + Other dust).

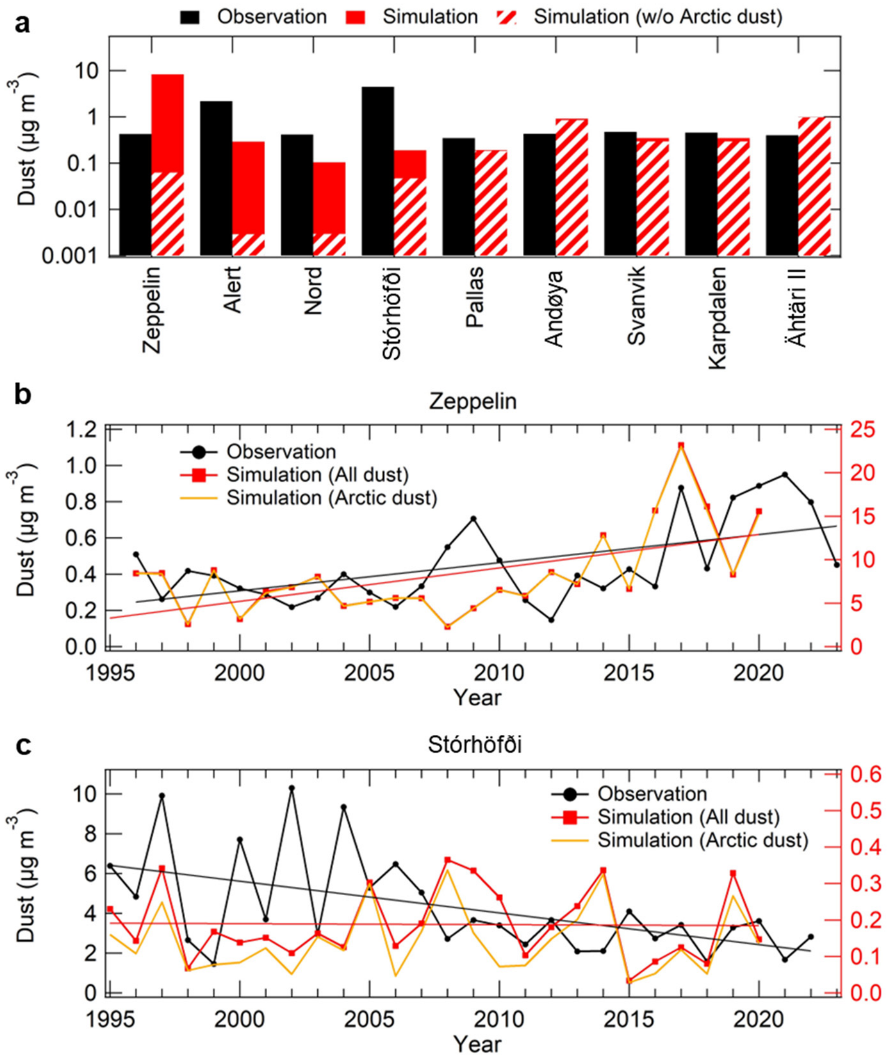

Supplementary Figure 3. Comparison of dust mass concentrations between surface observations and model simulations in the Arctic summer and fall. a, Period-averaged observed and simulated dust concentrations at nine sites (Methods). The filled and shaded areas indicate dust concentrations of Arctic dust and Other dust, respectively. **b−c,** Year-to-year variations of observed and simulated dust concentrations at (b) Zeppelin and (c) Stórhöfði with their trend lines. Summer and fall were chosen because the simulated amount of Arctic dust is high in these seasons (Fig. 4).

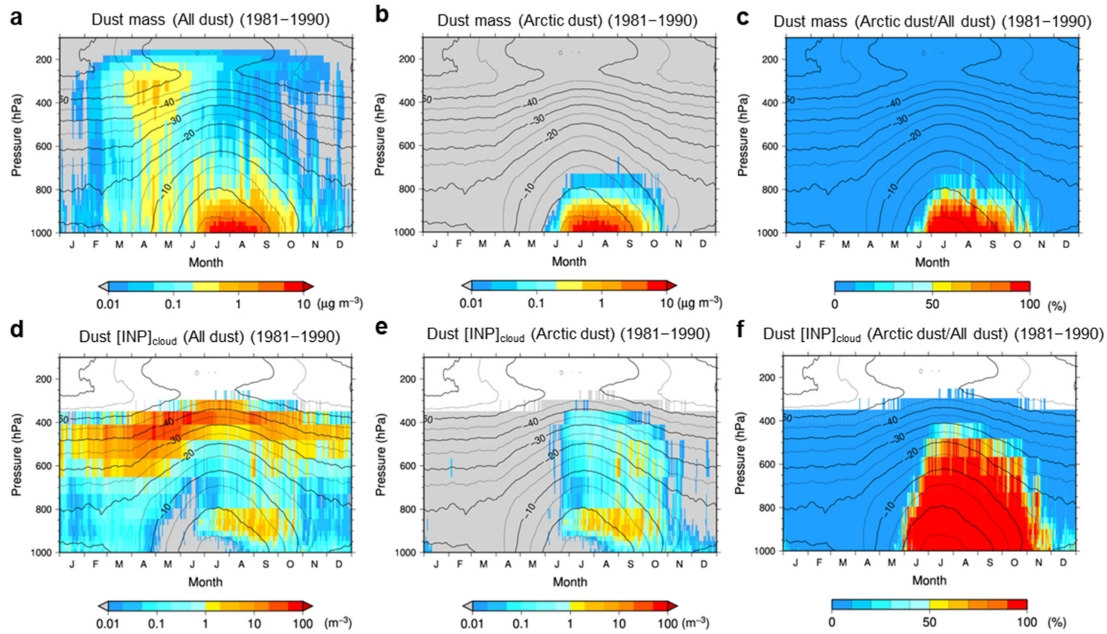

Supplementary Figure 4. Vertical distributions and temporal variations of dust in the Arctic (>60°N) averaged for 1981−1990. a−c, The mass concentrations of **(a)** All (Arctic + Other) dust and **(b)** Arctic dust and **(c)** their mass ratio (Arctic dust/All dust). **d−f,** $[INP]_{cloud}$ of **(d)** All (Arctic + Other) dust and **(e)** Arctic dust and **(f)** their ratio (Arctic dust/All dust). Results of the Base simulation are shown.

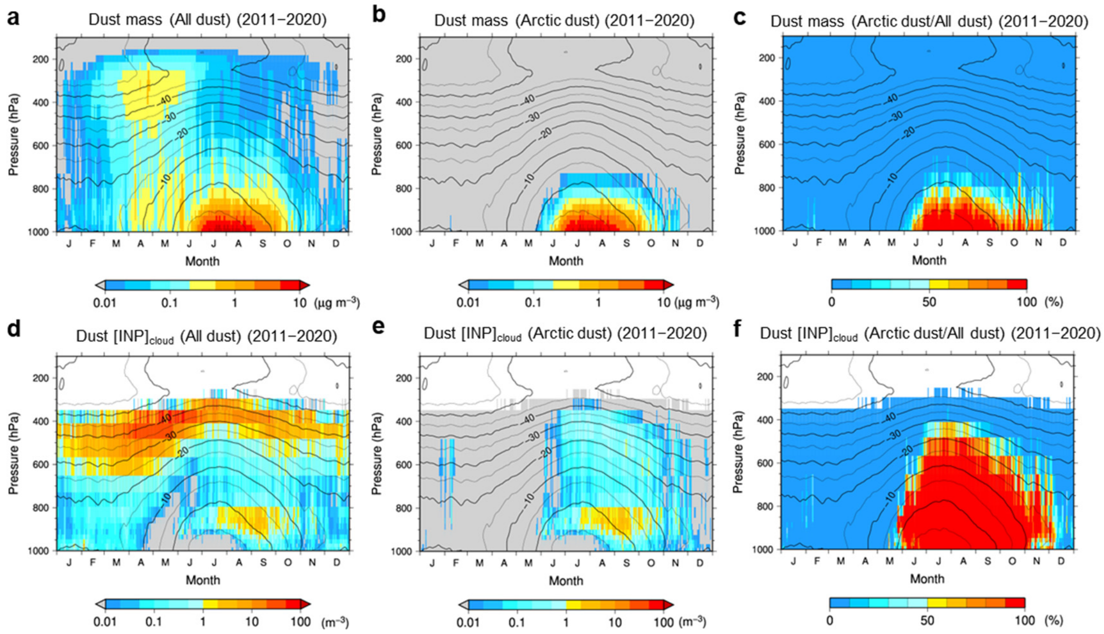

Supplementary Figure 5. Vertical distributions and temporal variations of dust in the Arctic (>60°N) averaged for 2011−2020. a−c, The mass concentrations of **(a)** All (Arctic + Other) dust and **(b)** Arctic dust and **(c)** their mass ratio (Arctic dust/All dust). **d−f,** $[INP]_{cloud}$ of **(d)** All (Arctic + Other) dust and **(e)** Arctic dust and **(f)** their ratio (Arctic dust/All dust). Results of the Base simulation are shown.

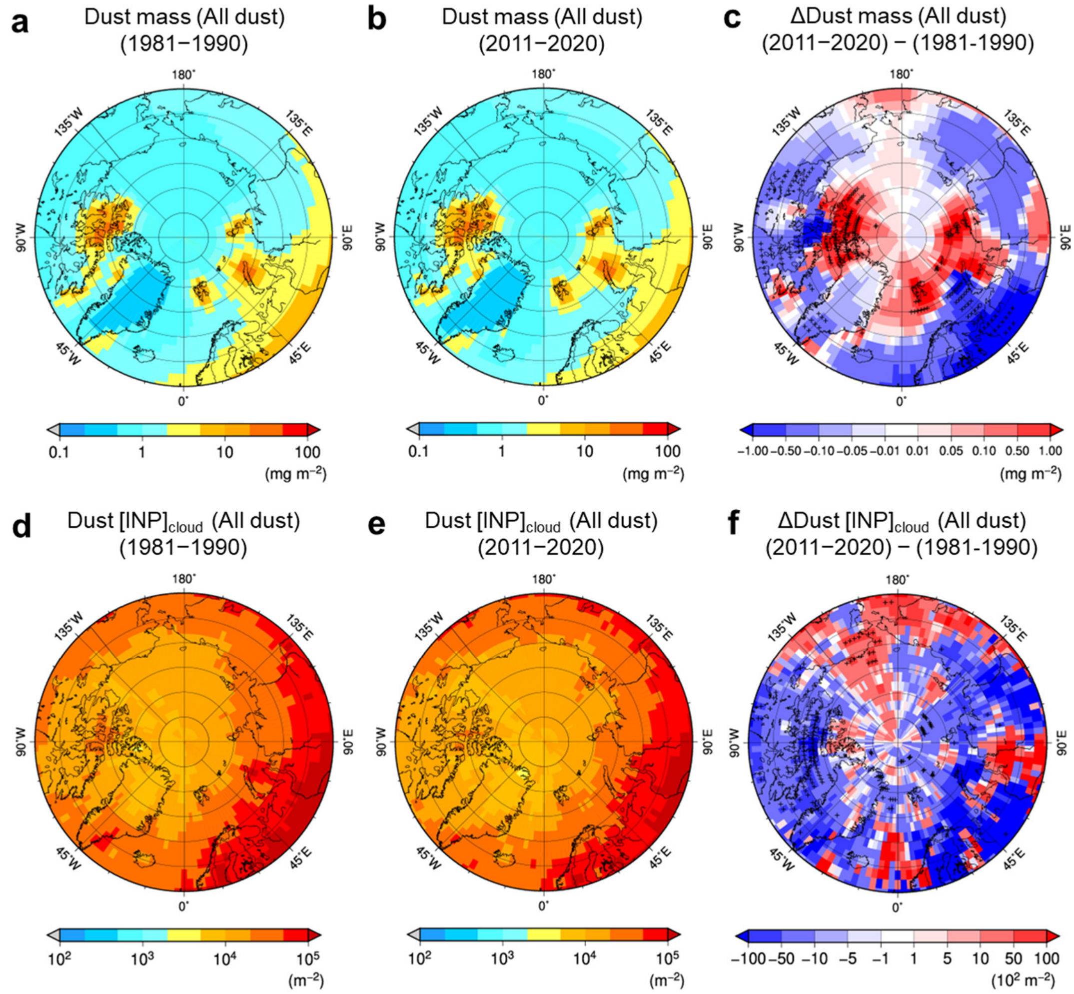

Supplementary Figure 6. Annual-mean vertically integrated mass and $[INP]_{cloud}$ of All (Arctic + Other) dust in the Arctic (>60°N). a−c, Vertically integrated mass concentrations for **(a)** 1981−1990 and **(b)** 2011−2020 and **(c)** their changes from 1981−1990 to 2011−2020. **d−f,** Vertically integrated $[INP]_{cloud}$ for **(d)** 1981−1990 and **(e)** 2011−2020 and **(f)** its changes from 1981−1990 to 2011−2020. **(c, f)** Regions with significant changes ($p<0.05$) from 1981−1990 to 2011−2020 are indicated by a + sign. Results of the Base simulation are shown.

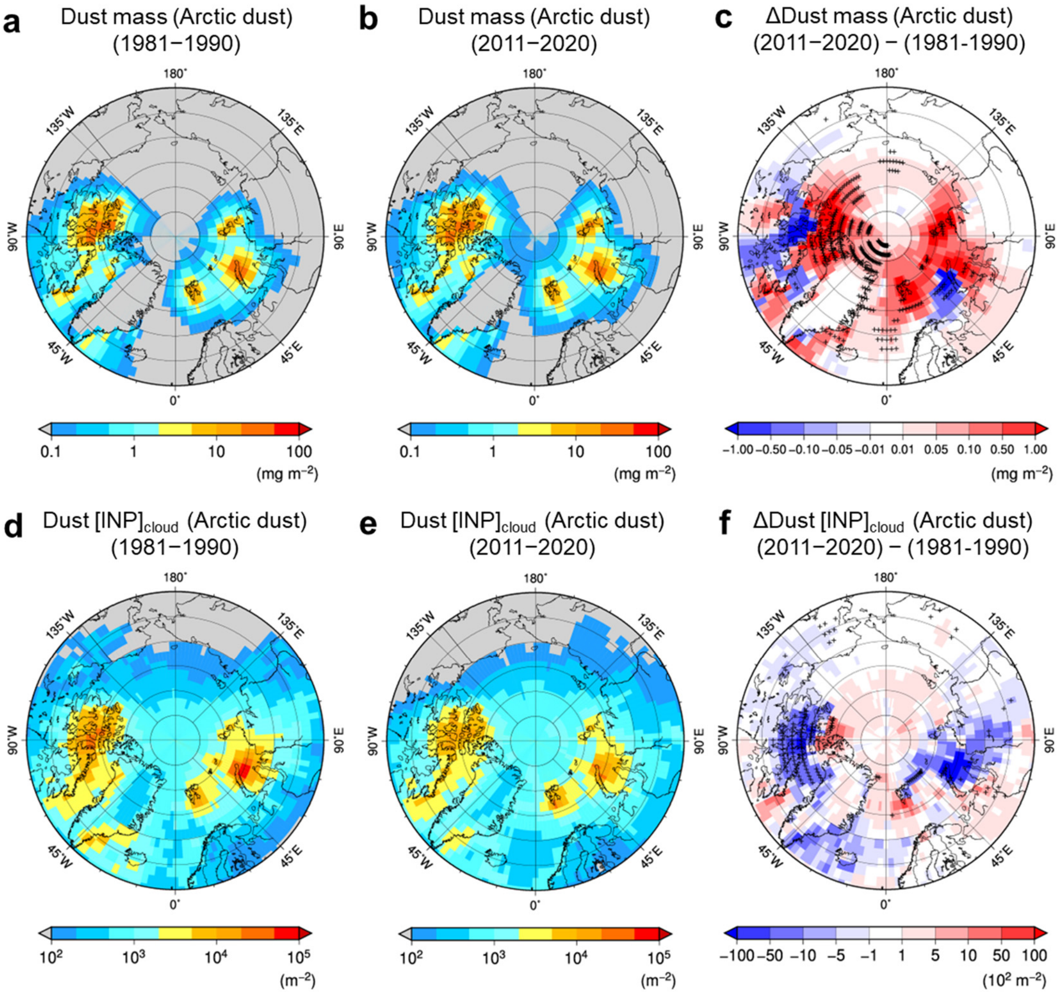

Supplementary Figure 7. Annual-mean vertically integrated mass and $[INP]_{cloud}$ of Arctic dust in the Arctic. a−c, Vertically integrated mass concentrations for **(a)** 1981−1990 and **(b)** 2011−2020 and **(c)** their changes from 1981−1990 to 2011−2020. **d−f,** Vertically integrated $[INP]_{cloud}$ for **(d)** 1981−1990 and **(e)** 2011−2020 and **(f)** its changes from 1981−1990 to 2011−2020. **(c, f)** Regions with significant changes ($p<0.05$) from 1981−1990 to 2011−2020 are indicated by a + sign. Results of the Base simulation are shown.

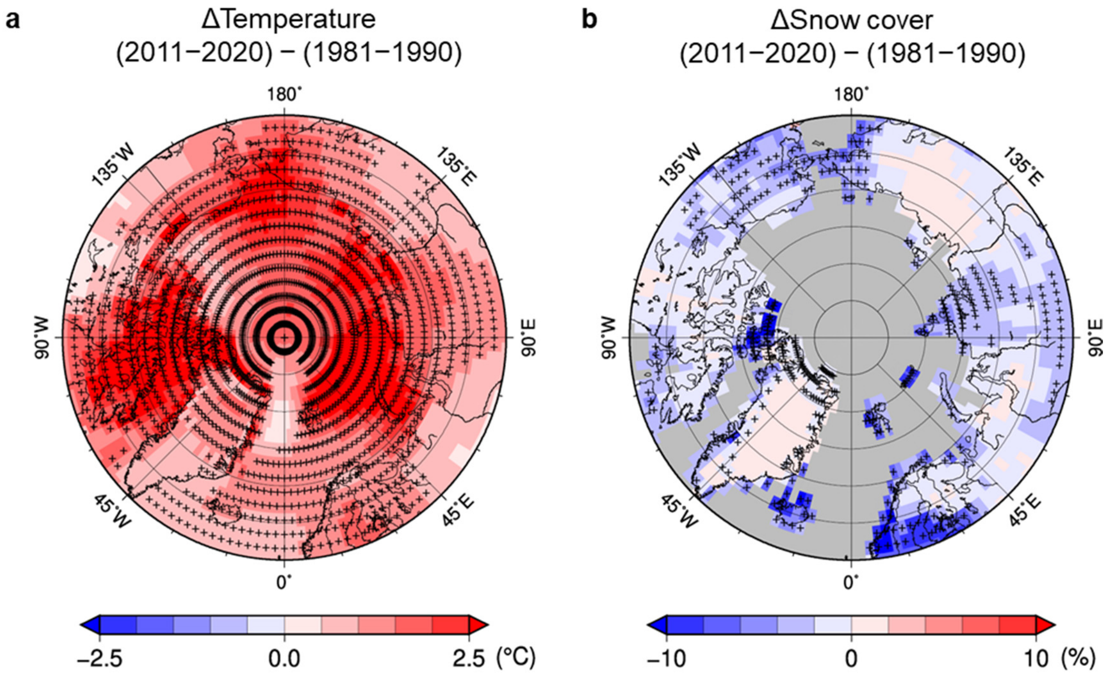

Supplementary Figure 8. Changes in surface air temperature and snow cover in the Arctic. Spatial distributions of changes in **(a)** surface air temperature and **(b)** snow cover in the Arctic from 1981−1990 to 2011−2020. Regions with significant changes (p<0.05) from 1981−1990 to 2011−2020 are indicated by a + sign.

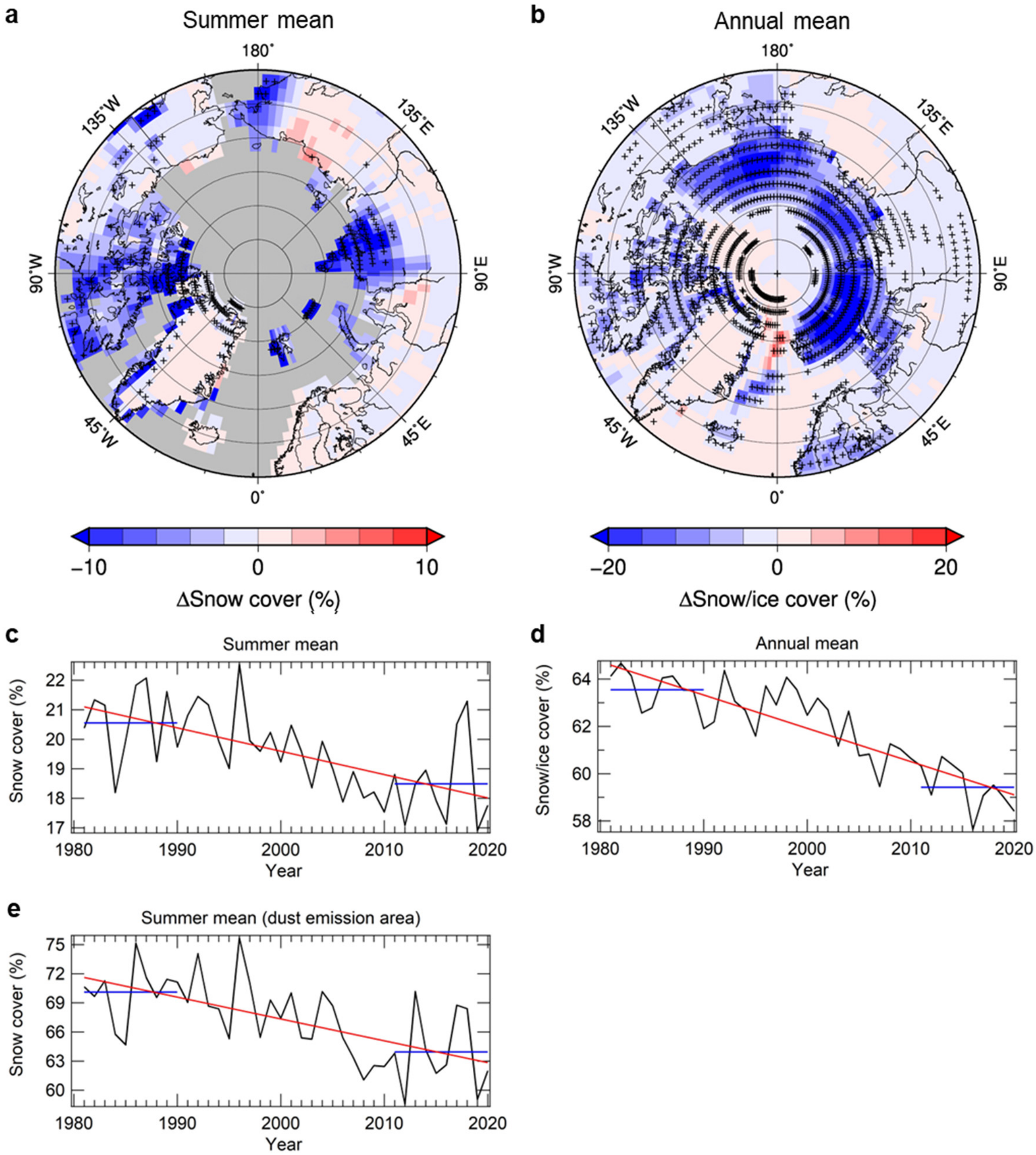

Supplementary Figure 9. Changes in snow and ice cover in the Arctic. a−b, Spatial distributions of changes in **(a)** summer-mean snow cover and **(b)** annual-mean snow/ice cover in the Arctic (>60°N) from 1981−1990 to 2011−2020. Regions with significant changes (p<0.05) from 1981−1990 to 2011−2020 are indicated by a + sign. **c−e,** Year-to-year variations of **(c, e)** summer-mean snow cover and **(d)** annual-mean snow/ice cover in the Arctic from 1981 to 2020. Snow cover is shown for **(c)** the percentage of the total land area of the Arctic and **(e)** the percentage of the area where Arctic dust is emitted. Red lines show the trends for 1981−2020, and blue lines show decadal averages for 1981−1990 and 2011−2020. Snow cover is derived from model simulations, and ice cover is based on the input data[5] used in the model.

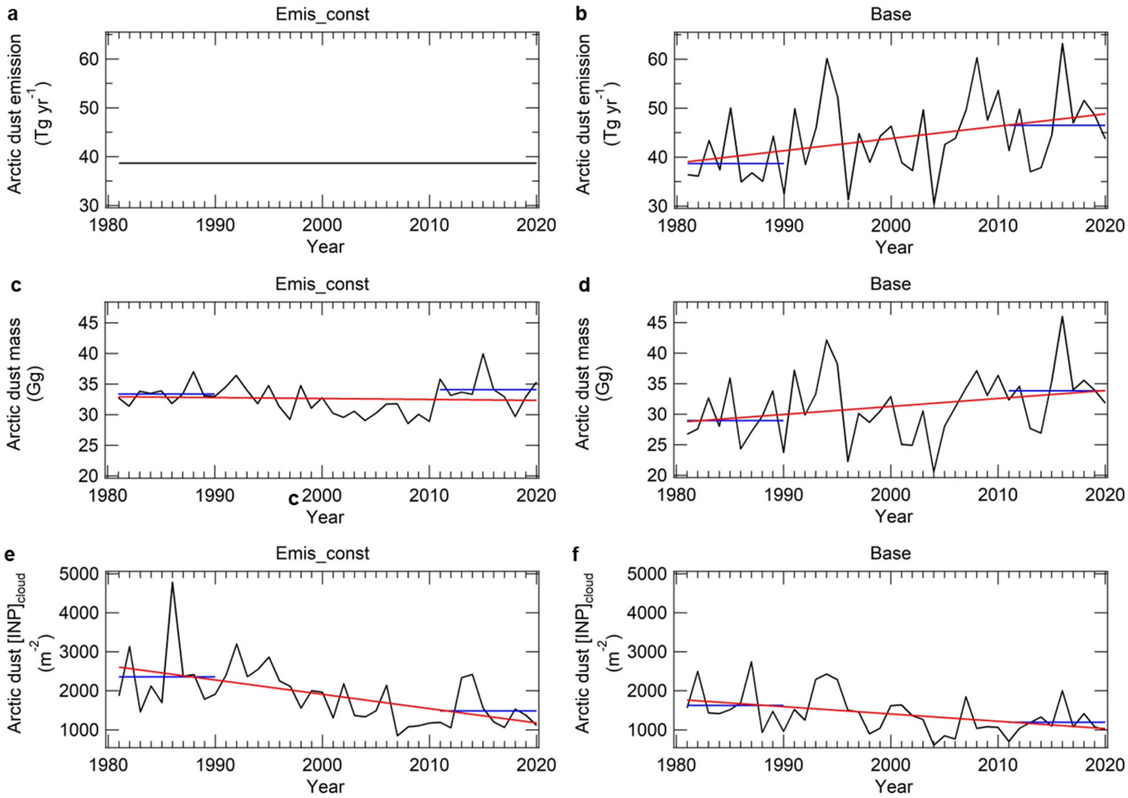

Supplementary Figure 10. Year-to-year variations of annual-mean Arctic dust and its $[INP]_{cloud}$ in the Arctic (>60°N). (a, b) The emission flux, **(c, d)** vertically integrated atmospheric burden, and **(e, f)** vertically integrated $[INP]_{cloud}$ of Arctic dust for **(a, c, e)** the Emis_const and **(b, d, f)** Base simulations. Red lines show the trends for 1981−2020, and blue lines show decadal averages for 1981−1990 and 2011−2020.

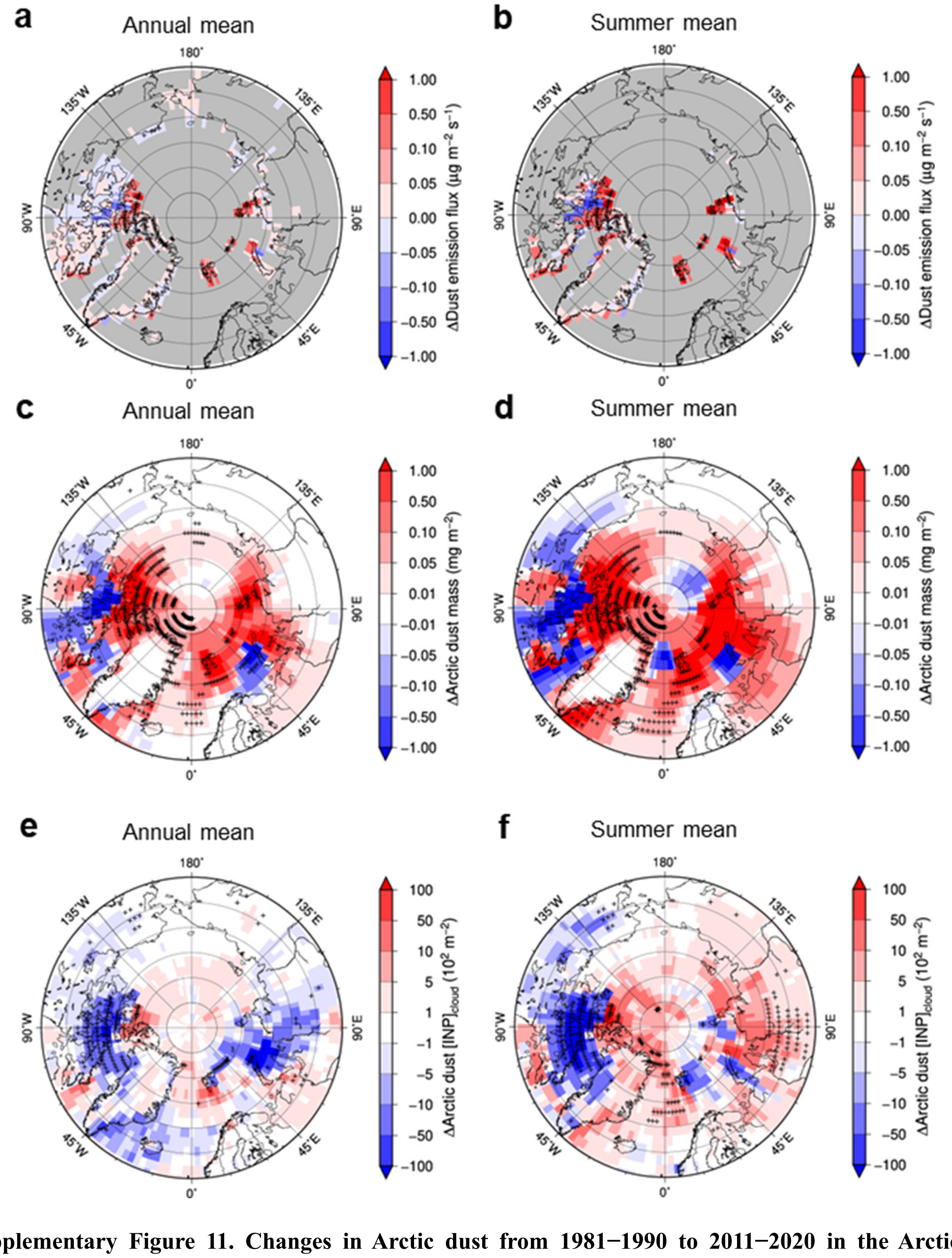

Supplementary Figure 11. Changes in Arctic dust from 1981−1990 to 2011−2020 in the Arctic. Changes in spatial distributions of **(a, c, e)** annual-mean and **(b, d, f)** summer-mean Arctic dust from 1981−1990 to 2011−2020 for **(a, b)** emission flux, **(c, d)** vertically integrated atmospheric burden, and **(e, f)** vertically integrated $[INP]_{cloud}$. Regions with significant changes (p<0.05) from 1981−1990 to 2011−2020 are indicated by a + sign. Results of the Base simulation are shown.

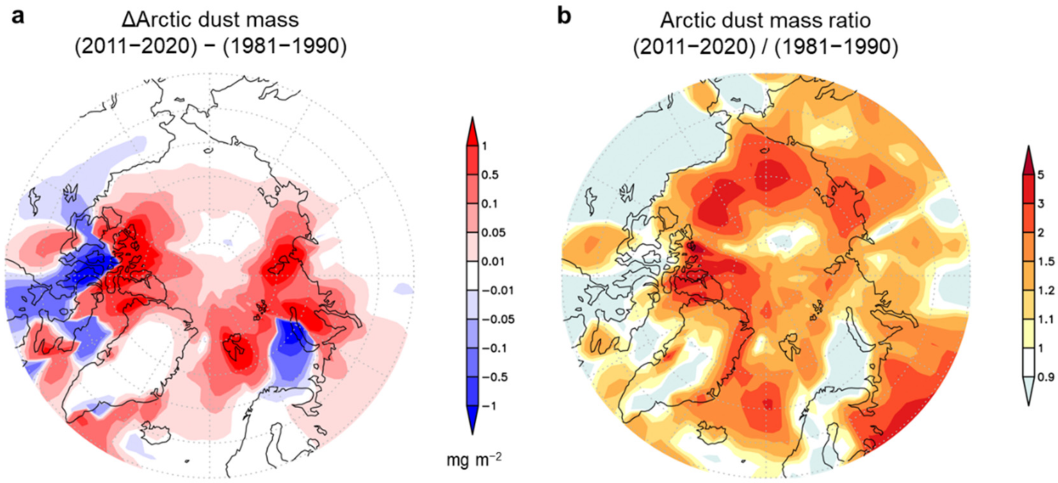

Supplementary Figure 12. Changes in vertically integrated Arctic dust mass concentrations in the Arctic. Spatial distributions of **(a)** the difference and **(b)** the ratio of vertically integrated Arctic dust mass concentrations from 1981−1990 to 2011−2020. Results of the Base simulation are shown.

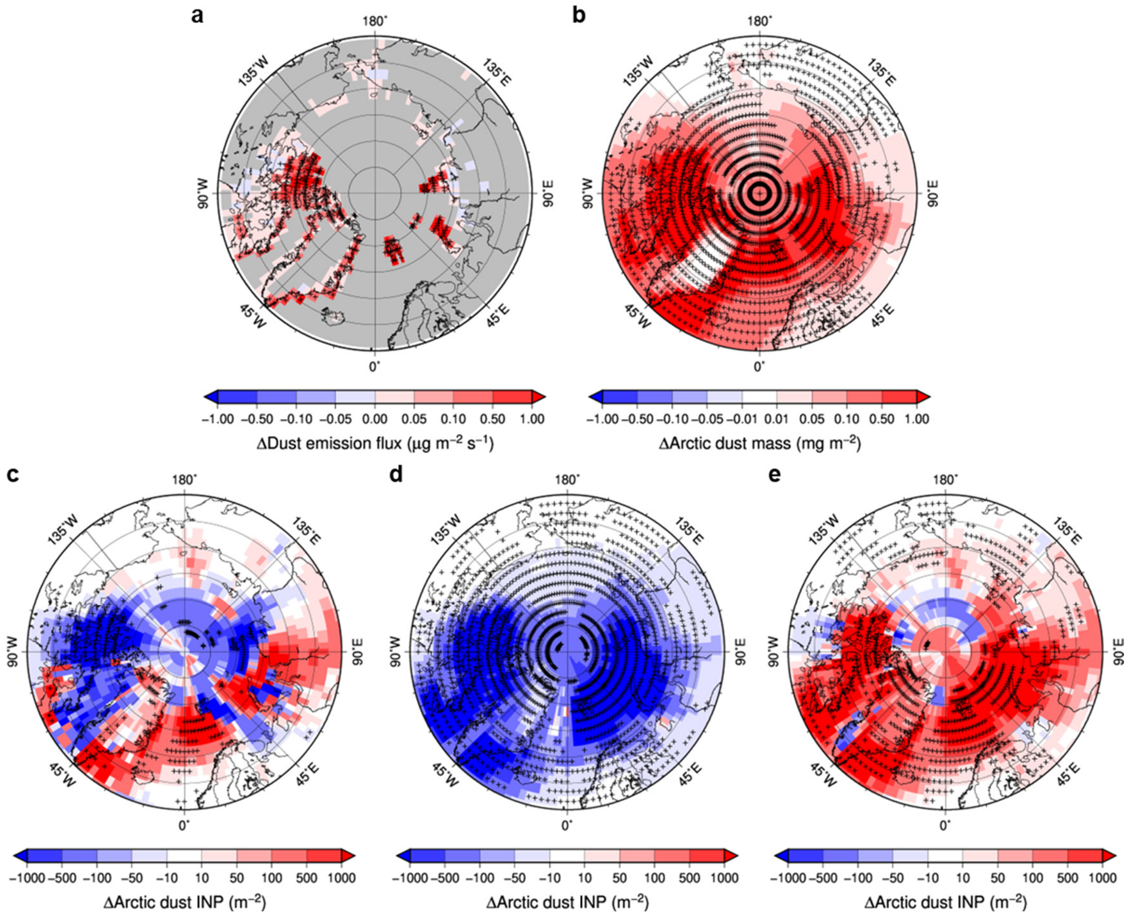

Supplementary Figure 13. Changes in decadal mean spatial distributions of Arctic dust with a 4 K increase in sea surface temperature (SST). a−b, Differences of annual-mean **(a)** emission flux and **(b)** vertically integrated mass concentrations between the case with uniformly increasing SST (by 4 K) and the case without the changing SST (using the present-day SST dataset in 2020). **c−e,** Changes in vertically integrated (>700 hPa) $[INP]_{cloud}$ during summer and fall between the 4 K increasing and present-day SST cases by **(c)** both the temperature and emission feedbacks, **(d)** the temperature feedback, and **(e)** the emission feedback. Regions with significant changes ($p<0.05$) between the 4 K increasing and present-day SST cases are indicated by a + sign.

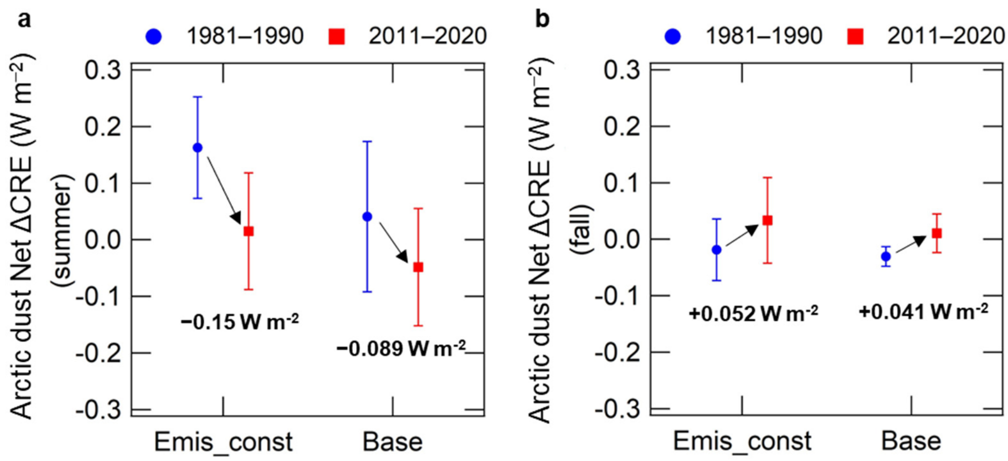

Supplementary Figure 14. Changes in net (shortwave + longwave) cloud radiative effect by Arctic dust $[INP]_{cloud}$ (ΔCRE) in the Arctic. Net ΔCRE in **(a)** summer and **(b)** fall in the Emis_const and Base simulations. Changes from 1981−1990 to 2011−2020 are also shown for each simulation. Error bars indicate standard deviations of interannual variability.

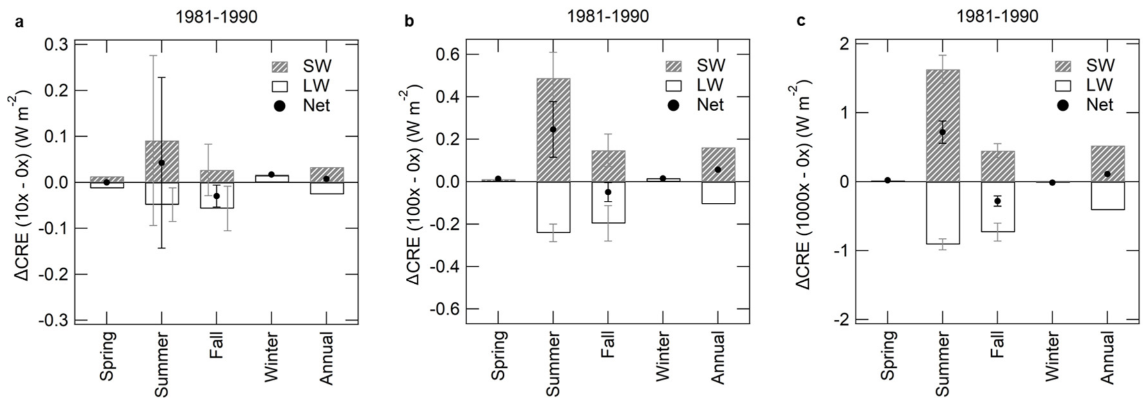

Supplementary Figure 15. Changes in cloud radiative effects by Arctic dust $[INP]_{cloud}$ (ΔCRE). a−b, Seasonal variations of shortwave (SW), longwave (LW), and net ΔCREs at the top of the atmosphere are shown for simulations with **(a)** 10-fold, **(b)** 100-fold, and **(c)** 1000-fold Arctic dust $[INP]_{cloud}$. Error bars indicate standard deviations of interannual variability.

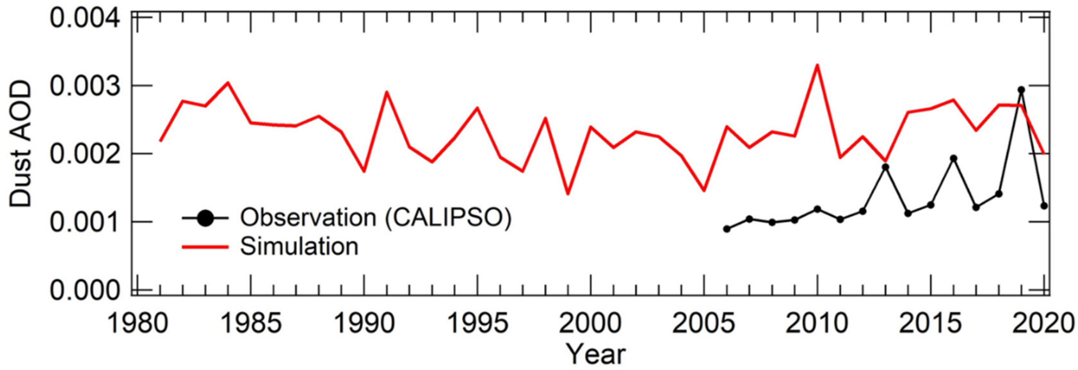

Supplementary Figure 16. Dust aerosol optical depth (AOD) in the Arctic summer and fall. Year-to-year variations are shown for CALIPSO observations (black) and model simulations (red).

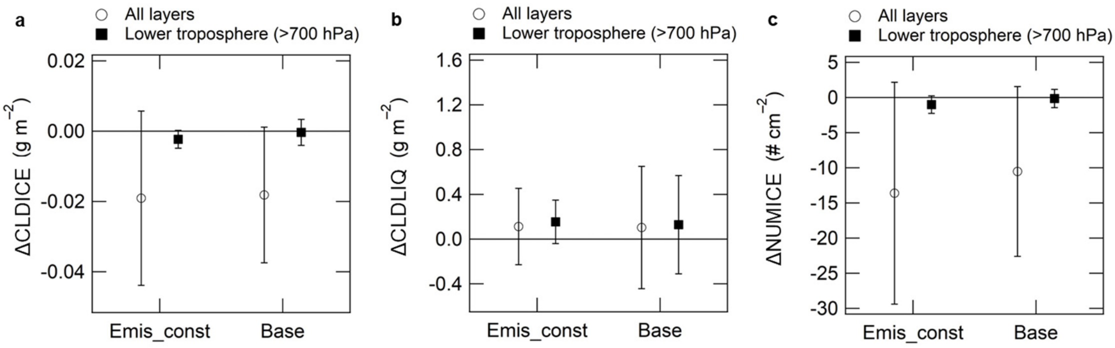

Supplementary Figure 17. Changes in the cloud water path in the Arctic (>60°N) by Arctic dust $[INP]_{cloud}$ from 1981−1990 to 2011−2020. Changes in **(a)** ice water path (IWP), **(b)** liquid water path (LWP), and **(c)** vertically integrated ice number concentrations in the Arctic from 1981−1990 to 2011−2020 are shown for the differences between simulations with 10× and 0× Arctic dust $[INP]_{cloud}$ (Methods). Open circles and closed squares show 10-year mean changes in IWP and LWP for all layers and in the lower troposphere (>700 hPa), respectively. Error bars indicate standard deviations of interannual variability. The Base simulation calculates interannual variations of Arctic dust emissions online, whereas the Emis_const simulation has no interannual variations of Arctic dust emissions (see Methods).

Supplementary Tables

Supplementary Table 1. Summary of simulated dust statistics in the Arctic (>60°N) for the Emis_const simulation

Parameter	Source [a]	Unit	1981−1990 [b]	2011−2020 [b]	(2011−2020) – (1981−1990)
Annual mean					
Surface temperature	---	°C	−9.5±0.35	−7.8±0.51	1.6
Snow/Ice cover	---	%	64±0.87	59±0.97	−4.1
Emission	Arctic dust	Tg yr^{-1}	39±0	39±0	0
Burden (all layers)	Arctic dust	Gg	33±1.5	34±2.6	0.72 (+2.2%)
	All dust	Gg	72±7.8	68±4.7	−4.1
Burden (>700hPa)	Arctic dust	Gg	33±1.5	34±2.6	0.73 (+2.2%)
	All dust	Gg	45±2.6	44±2.9	−0.83
$[INP]_{cloud}$ (all layers)	Arctic dust	# m^{-2}	2356±974	1483±505	−873 (−37%)
	All dust	# m^{-2}	34170±4882	30662±3596	−3508
$[INP]_{cloud}$ (>700hPa)	Arctic dust	# m^{-2}	1351±348	848±337	−502 (−37%)
	All dust	# m^{-2}	1462±335	956±359	−506
Summer mean					
Surface temperature	---	°C	5.0±0.31	5.9±0.40	0.91
Snow/Ice cover	---	%	34±1.4	29±1.4	−4.6
Emission	Arctic dust	Tg $season^{-1}$	31±0	31±0	0
Burden (all layers)	Arctic dust	Gg	106±7.0	112±9.6	5.5 (+5.2%)
	All dust	Gg	150±12	148±11	−2.2
Burden (>700hPa)	Arctic dust	Gg	106±7.0	112±9.6	5.4 (+5.1%)
	All dust	Gg	123±8.7	127±8.4	3.3
$[INP]_{cloud}$ (all layers)	Arctic dust	# m^{-2}	2759±752	2123±614	−636 (−23%)
	All dust	# m^{-2}	45584±9973	35070±6700	−10514
$[INP]_{cloud}$ (>700hPa)	Arctic dust	# m^{-2}	1678±478	1086±414	−591 (−35%)
	All dust	# m^{-2}	1679±478	1087±414	−592

[a] Arctic dust is defined as dust emitted from north of 60°N. All dust is the sum of Arctic dust and Other dust (emitted from south of 60°N).
[b] Decadal averages and standard deviations of interannual variability are shown.

Supplementary Table 2. Summary of simulated dust statistics in the Arctic (>60°N) for the Base simulation

Parameter	Source [a]	Unit	1981−1990 [b]	2011−2020 [b]	(2011−2020) – (1981−1990)
Annual mean					
Surface temperature	---	°C	−9.5±0.35	−7.8±0.51	1.6
Snow/Ice cover	---	%	64±0.87	59±0.97	−4.1
Emission	Arctic dust	Tg yr^{-1}	39±5.4	46±7.6	7.8 (+20%)
Burden (all layers)	Arctic dust	Gg	29±4.0	34±5.2	4.9 (+17%)
	All dust	Gg	67±9.8	67±5.8	−0.23
Burden (>700hPa)	Arctic dust	Gg	29±4.0	34±5.2	4.9 (+17%)
	All dust	Gg	40±4.7	44±5.1	3.4
$[INP]_{cloud}$ (all layers)	Arctic dust	# m^{-2}	1622±584	1191±344	−431 (−27%)
	All dust	# m^{-2}	33510±5159	30399±3280	−3111
$[INP]_{cloud}$ (>700hPa)	Arctic dust	# m^{-2}	892±336	683±249	−209 (−23%)
	All dust	# m^{-2}	1003±348	791±256	−212
Summer mean					
Surface temperature	---	°C	5.0±0.31	5.9±0.40	0.91
Snow/Ice cover	---	%	34±1.4	29±1.4	−4.6
Emission	Arctic dust	Tg season^{-1}	31±3.6	38±5.6	6.8 (+22%)
Burden (all layers)	Arctic dust	Gg	94±13	111±17	18 (+19%)
	All dust	Gg	138±16	148±18	10
Burden (>700hPa)	Arctic dust	Gg	94±13	111±16	18 (+19%)
	All dust	Gg	111±14	126±17	16
$[INP]_{cloud}$ (all layers)	Arctic dust	# m^{-2}	2650±886	2295±1025	−355 (−13%)
	All dust	# m^{-2}	45595±10137	35425±6396	−10170
$[INP]_{cloud}$ (>700hPa)	Arctic dust	# m^{-2}	1563±620	1130±687	−433 (−28%)
	All dust	# m^{-2}	1564±620	1130±687	−434

[a] Arctic dust is defined as dust emitted from north of 60°N. All dust is the sum of Arctic dust and Other dust (emitted from south of 60°N).

[b] Decadal averages and standard deviations of interannual variability are shown.

Supplementary Note 1: Validation of model simulations

We have validated our simulations for dust and its role as INPs in our previous studies[6–9] and improved the agreement of INP number concentrations in the Arctic between observations and model simulations by considering the high ice nucleating ability of Arctic dust[6]. Arctic dust emission in this study is estimated to be 46 Tg y^{-1} (>60°N for 2011−2020), which is generally consistent with that estimated in Groot Zwaaftink et al.[10] (48 Tg y^{-1} from >60°N). The contribution of Arctic dust emission to global dust emission is 1.3% (for 2011−2020), which is also within the range in previous estimates of 0.6−5%[1,10–12].

Ice core observations[4] at the Southeastern Dome (SE-Dome) in Greenland showed an increase in dust deposition flux from 1960 to 2014, and Amino et al.[4] suggested that an important reason for this is an increase in local dust emissions due to increasing temperatures and snow-free areas in Greenland. This ice core has the advantageous feature of a high-precision timescale with an error of less than 2 months, and to our knowledge, this is the only ice core data that can provide dust deposition flux in the Arctic with seasonal resolution from the 1980s to the 2010s. In summer (June−August) and fall (September−November), when Arctic dust emissions are high, the simulated dust deposition flux at this site is overestimated by a factor of more than several times in some years (1990, 1991, 1994, and 2009), but it is consistent with the observed dust deposition flux within a factor of 3 for 29 years out of 34 years (Supplementary Fig. 2). The observed mean dust deposition flux in summer and fall increases by 85% from 1981−1990 (2.3 mg m^{-2} $month^{-1}$) to 2005−2014 (4.3 mg m^{-2} $month^{-1}$; the last 10 years of the ice core observations), with an increasing trend of 0.96 ± 0.25 mg m^{-2} $decade^{-1}$. The simulated mean deposition flux of All dust (Arctic dust + Other dust) does not increase during this period, but when we exclude the year 1990, which has extremely high dust deposition flux, the simulated flux in summer and fall increases by 41% from 1981−1989 (3.1 mg m^{-2} $month^{-1}$) to 2005−2014 (4.4 mg m^{-2} $month^{-1}$), with a trend of 0.39 ± 0.38 mg m^{-2} $decade^{-1}$. The simulated deposition flux of the Arctic dust in summer and fall also increases by 37% during this period, with a trend of 0.43 ± 0.28 mg m^{-2} $decade^{-1}$ (Supplementary Fig. 2). The contribution of Arctic dust to All dust of about 45% for both 1981−1989 and 2005−2014. These results show that the model simulations roughly reproduce the observed dust deposition flux and its increasing trend during the simulation periods, while overestimating the amount of the dust deposition flux for some years. The extremely high deposition flux in 1990 in the model simulation is due to the transport of a plume with high dust concentrations from Europe to Greenland on 29 July 1990. This dust event is the largest in the past 40 years in the model, with a deposition flux about five times higher than other dust events calculated every several years. However, the extremely high dust deposition was not recorded in the ice core data in 1990, suggesting that the magnitude of the dust event on this day was much smaller in the real atmosphere. In addition, the possibility also remains that this dust plume was not efficiently transported to the SE-Dome and hence might not be preserved well in the ice core. Excluding the deposition flux on 29 July 1990, the simulated dust deposition flux in 1990 decreases from 24 mg m^{-2} $month^{-1}$ to 5.5 mg m^{-2} $month^{-1}$, which is consistent with the ice core observations within a factor of 2.

We also used surface observations of aluminum in the EBAS database to compare observed and simulated dust mass concentrations at nine sites in the Arctic (Methods; Supplementary Fig. 3). At the sites in and around Greenland (Alert, Nord, and

Stórhöfði), the model underestimates the observed dust mass concentrations in summer and fall. The simulated Other dust concentrations at these sites are very low (<0.1 μg m^{-3}) in summer and fall, and the agreement with the observations is greatly improved by considering Arctic dust (Supplementary Fig. 3a). At Zeppelin, the simulated Other dust concentrations underestimate the observed dust concentrations by about an order of magnitude, while the simulated dust concentrations including both Arctic and Other dust overestimate them by more than an order of magnitude (Supplementary Fig. 3a). This overestimation is consistent with the overestimation of INP number concentrations at Zeppelin shown by Kawai et al.[6] At the sites in and around the Scandinavian peninsula (Pallas, Andøya, Svanvik, Karpdalen, and Ähtäri II), the contribution of Arctic dust is small (<15%), and the simulated Other dust concentrations roughly reproduce the observed dust concentrations (Supplementary Fig. 3a). Of these observation sites, Zeppelin and Stórhöfði have long-term data spanning more than 20 years. At Zeppelin, dust mass concentrations in summer and fall show an increasing trend in both observations (0.15 ± 0.045 μg m^{-3} $decade^{-1}$) and model simulations (3.8 ± 1.1 μg m^{-3} $decade^{-1}$), although the absolute mass concentrations are overestimated by the model (Supplementary Fig. 3b). In contrast, at Stórhöfði in Iceland, there is no increase in either observed or simulated dust mass concentrations since 1995 because the contribution of Arctic dust is small in the model (Supplementary Fig. 3c).

The dust aerosol optical depth (AOD) from CALIPSO in the Arctic in summer is about 0.001−0.002 (at 532 nm) (Supplementary Fig. 16). The detection of dust by CALIPSO in the Arctic may include large uncertainty given the low dust AOD values. However, the simulated dust AOD (at 550 nm) is in reasonable agreement (within a factor of 2) with the CALIPSO dust AOD in the Arctic.

In our simulations, the annual mean liquid water path (LWP) in the Arctic for 2011−2020 is 49 g m^{-2}, which is generally consistent with the LWPs (30−81 g m^{-2}) in the reanalysis data (M2Modis, MERRA, MERRA2, ERA5, ERA-Interim, and JRA-55)[13]. The annual mean ice water path (IWP) in the Arctic is 11 g m^{-2}, which is generally consistent with the IWPs estimated in MERRA and MERRA2 (13−15 g m^{-2}), but lower than the IWPs in the other reanalysis products (22−59 g m^{-2})[12]. This result suggests that our model simulations may underestimate the IWP and ice fraction in the Arctic and that the liquid-to-ice conversion by primary ice nucleation might also be underestimated.

Supplementary Note 2: Uncertainties in ΔCRE estimates

There are large uncertainties in the estimates of the changes in CREs by the Arctic dust $[INP]_{cloud}$ (ΔCRE) from 1981−1990 to 2011−2020. For example, estimates of ice nucleating ability and INP concentrations generally have uncertainties of one or two orders of magnitude. There are also large uncertainties in the response of clouds (e.g., LWP) to INPs. As described in Supplementary Note 1, the IWP and the ice fraction in the Arctic in our model are lower than previous estimates[13]. A recent study[14] reported that the LWP change in the Arctic caused by INPs in the Arctic is on the order of 0.1−1 g m^{-2}. In our simulations, the changes in LWP by including Arctic dust $[INP]_{cloud}$ are about 0.1 g m^{-2} and small especially in the lower troposphere (Supplementary Fig. 17). Possible causes of the small change in ice water content in the lower troposphere are the higher temperature in the lower troposphere than in the upper troposphere and the faster removal rate of ice compared to that of liquid water.

Furthermore, changes in the cloud phase and ΔCRE by the Arctic dust $[INP]_{cloud}$

strongly depend on the model's treatment of the conversion of liquid droplets to ice crystals (e.g., the Wegener-Bergeron-Findeisen process)[14–16]. ΔCRE may also be influenced significantly by the estimation of the Other dust $[INP]_{cloud}$, which are abundant in the middle and upper troposphere in the Arctic. To better constrain the ΔCRE change, it may be necessary to validate the Other dust $[INP]_{cloud}$ in addition to further improving the estimation of Arctic dust and its ice nucleating ability. In addition, this study considers only dust as aerosols acting as INPs, but in the real atmosphere, other aerosol species such as bioaerosols, organic aerosols from oceans, and black carbon also act as INPs[17–26]. This study also assumes the same ice nucleating ability for all Arctic dust, but the ice nucleating ability of Arctic dust might differ depending on where and how it is emitted[27–31]. INPs from non-dust species and the diversity of ice nucleating ability of Arctic dust should be considered in future modeling studies for better simulations of $[INP]_{cloud}$, primary ice nucleation, and their impacts on clouds and ΔCRE changes.

Considering such uncertainties in INPs and the possibility of the underestimation of ice formation in our model, our ΔCRE estimates have large uncertainties.

Supplementary References

1. Tobo, Y. *et al.* Glacially sourced dust as a potentially significant source of ice nucleating particles. *Nat. Geosci.* **12**, 253−258 (2019).
2. DeMott, P. J. *et al.* Integrating laboratory and field data to quantify the immersion freezing ice nucleation activity of mineral dust particles. *Atmos. Chem. Phys.* **15**, 393−409 (2015).
3. Kok, J. F. A scaling theory for the size distribution of emitted dust aerosols suggests climate models underestimate the size of the global dust cycle. *Proc. Natl. Acad. Sci. U.S.A.* **108**, 1016−1021 (2011).
4. Amino, T. *et al.* Increasing dust emission from ice free terrain in southeastern Greenland since 2000. *Polar Sci.* **27**, 100599 (2021).
5. Hurrell, J. W. *et al.* A new sea surface temperature and sea ice boundary dataset for the Community Atmosphere Model. *J. Clim.* **21**, 5145−5153 (2008).
6. Kawai, K., Matsui, H. & Tobo, Y. Dominant role of Arctic dust with high ice nucleating ability in the Arctic lower troposphere. *Geophys. Res. Lett.* **50**, e2022GL102470 (2023).
7. Matsui, H. & Mahowald, N. M. Development of a global aerosol model using a two-dimensional sectional method: 2. Evaluation and sensitivity simulations. *J. Adv. Model. Earth Syst.* **9**, 1887−1920 (2017).
8. Liu, M. & Matsui, H. Aerosol radiative forcings induced by substantial changes in anthropogenic emissions in China from 2008 to 2016. *Atmos. Chem. Phys.* **21**, 5965−5982 (2021).
9. Kawai, K., Matsui, H. & Tobo, Y. High potential of Asian dust to act as ice nucleating particles in mixed-phase clouds simulated with a global aerosol-climate model. *J. Geophys. Res. Atmos.* **126**, e2020JD034263 (2021).
10. Groot Zwaaftink, C. D., Grythe, H., Skov, H. & Stohl, A. Substantial contribution of northern high-latitude sources to mineral dust in the Arctic. *J. Geophys. Res. Atmos.* **121**, 13678−13697 (2016).
11. Bullard, J. E. *et al.* High-latitude dust in the Earth system. *Rev. Geophys.* **54**, 447−485 (2016).
12. Bullard, J. E. The distribution and biogeochemical importance of high-latitude dust in the Arctic and Southern Ocean-Antarctic regions. *J. Geophys. Res. Atmos.* **122**, 3098−3103 (2017).
13. Gu, M., Wang, Z., Wei, J. & Yu, X. An assessment of Arctic cloud water paths in atmospheric reanalysis. *Acta Oceanol. Sin.* **40**, 46−57 (2021).
14. Shi, Y. *et al.* Relative importance of high-latitude local and long-range-transported dust for Arctic ice-nucleating particles and impacts on Arctic mixed-phase clouds. *Atmos. Chem. Phys.* **22**, 2909−2935 (2022).
15. Zhang, Y. *et al.* Evaluation of clouds in version 1 of the E3SM atmosphere model with satellite simulators, *J. Adv. Model. Earth Syst.*, **11**, 1253−1268 (2019).
16. Zhang, Y. *et al.* Toward understanding the simulated phase partitioning of Arctic single-layer mixed-phase clouds in E3SM, *Earth Space Sci.*, **7**, e2020EA001125 (2020).
17. Wilson, T. W. *et al.* A marine biogenic source of atmospheric ice-nucleating particles. *Nature* **525**, 234−238 (2015).

18. Wex, H. *et al.* Intercomparing different devices for the investigation of ice nucleating particles using Snomax® as test substance. *Atmos. Chem. Phys.* **15**, 1463−1485 (2015).
19. Hoose, C., Kristjánsson, J. E. & Burrows, S. M. How important is biological ice nucleation in clouds on a global scale? *Environ. Res. Lett.* **5**, 024009 (2010).
20. Tobo, Y. *et al.* Biological aerosol particles as a key determinant of ice nuclei populations in a forest ecosystem. *J. Geophys. Res. Atmos.* **118**, 10100−10110 (2013).
21. Spracklen, D. V. & Heald, C. L. The contribution of fungal spores and bacteria to regional and global aerosol number and ice nucleation immersion freezing rates. *Atmos. Chem. Phys.* **14**, 9051−9059 (2014).
22. O'Sullivan, D. *et al.* Contributions of biogenic material to the atmospheric ice-nucleating particle population in North Western Europe. *Sci. Rep.* **8**, 13821 (2018).
23. Creamean, J. M. *et al.* Ice nucleating particles carried from below a phytoplankton bloom to the Arctic atmosphere. *Geophys. Res. Lett.* **46**, 8572−8581 (2019).
24. Creamean, J. M. *et al.* Thawing permafrost: an overlooked source of seeds for Arctic cloud formation. *Environ. Res. Lett.* **15**, 084022 (2020).
25. Schill, G. P. *et al.* The contribution of black carbon to global ice nucleating particle concentrations relevant to mixed-phase clouds. *Proc. Natl. Acad. Sci. U.S.A.* **117**, 22705−22711 (2020).
26. Ickes, L. *et al.* The ice-nucleating activity of Arctic sea surface microlayer samples and marine algal cultures. *Atmos. Chem. Phys.* **20**, 11089−11117 (2020).
27. Sanchez-Marroquin, A. *et al.* Iceland is an episodic source of atmospheric ice-nucleating particles relevant for mixed-phase clouds. *Sci. Adv.* **6**, eaba8137 (2020).
28. Xi, Y. *et al.* Ice nucleating properties of airborne dust from an actively retreating glacier in Yukon, Canada. *Environ. Sci. Atmos.* **2**, 714−726 (2022).
29. Creamean, J. M. *et al.* Annual cycle observations of aerosols capable of ice formation in central Arctic clouds. *Nat. Commun*. **13**, 3537 (2022).
30. Li, G., Wieder, J., Pasquier, J. T., Henneberger, J. & Kanji, Z. A. Predicting atmospheric background number concentration of ice-nucleating particles in the Arctic. *Atmos. Chem. Phys.* **22**, 14441–14454 (2022).
31. Sze, K. C. *et al.* Ice-nucleating particles in northern Greenland: annual cycles, biological contribution and parameterizations. *Atmos. Chem. Phys.* **23**, 4741–4761 (2023).